THERMAL ANALYSIS OF A SERPENTINE FLAT PLATE COLLECTOR AND INVESTIGATION OF THE FLOW AND CONVECTION REGIME

by

Dimitrios N. KORRES [*] ***and Christos TZIVANIDIS***
National Technical University of Athens, Athens, Greece

Original scientific paper
https://doi.org/10.2298/TSCI161130172K

A special kind of flat plate collectors was examined in detail through CFD analysis. The distinctiveness of the current model has to do with the piping system was applied which is a serpentine flow conduit. The operation of the collector was examined at four different inclination angles (0°, 15°, 30°, and 45°) and several values of the inlet water temperature (10-80 °C per 10 °C) by providing the same heat perpendicular to the cover in each case. The thermal efficiency as well as the temperature fields of the collector was determined first. Furthermore, the overall heat losses were calculated and compared to these arisen from the Cooper-Dunkle assumption while the mean divergence between these two solutions was around 5%. Moreover, the natural convection inside the gap as well as the tube to water convection was examined and the heat transfer coefficients were validated from theoretical models in horizontal position. In particular, the simulation results found to diverge from the theoretical ones about 12.5% and 7% as regards the pipe flow and the air-gap, respectively. In addition, a remarkable flow phenomenon was observed at the bends of the pipe and the nature of it was explained in detail. Last but not least, the inclination angle seems that affects significantly the collector's performance since the higher the slope the lower the convection losses. Solidworks and its simulation program Flow Simulation were used to design and simulate the whole collector.

Key words: *Solidworks, Flow Simulation, serpentine, efficiency, natural convection, slope, secondary flows*

Introduction

A significant proportion of the energy consumed for fulfilling needs of modern societies is being covered from solar energy via a big range of systems. The simplest of them is the solar domestic hot water system and the most economical way to implement it is to use flat plate collectors (FPC).

An FPC is a special form of heat exchanger that collects the heat coming from the Sun in the form of radiation through a highly absorptive surface and conveys it into the working medium. The last one (water, air, oil) circulates either naturally or forcibly and can be used directly for consumption, for space heating, in an absorption cooling cycle or finally goes into a secondary heat exchanger where it conveys its heat to the fluid we want to warm up. Greenhouse effect takes place in the collector's spacing resulting in the entrapment of the long wave (thermal) radiation. Some of the incident (high frequency) solar radiation is being reflected from the plate

* Corresponding author, e-mail: korres@central.ntua.gr

and converted into low frequency radiation which combined with the emitted from the plate one goes mainly to the cover. Given the cover's opacity to such radiation the largest portion of it returns to the absorber [1-4].

There are many different *plate-tube* systems that can be applied on an FPC, however, the most well-known is the *Riser-Header* one as well as the *Serpentine* system. The main difference between these two configurations is the way that the fluid-flows in the tubes. In the *Riser- Header* system we first have separation of the flow (from the cold header tube to the risers) and then reunification (from the risers to the hot header). The *Serpentine* system is an one-pipe application that allows higher fluid temperature differences, due to the fact that the water stays more in the collector given the greater tube length which can be implemented, ensuring a lower cost piping geometry for the same external dimensions of the FPC where can be applied, compared to the *Riser-Header* system.

Hence, the Serpentine flow system is of considerable interest and we are going to look at it in detail.

There are just a few studies have conducted in how such application works. For instance, Eisenmann *et al.* [5] conducted experimental research to investigate the performance of serpentine FPC. The CFD analysis through ANSYS has, also, been conducted by Cook [6] for the determination of the water temperature fields of a serpentine collector. The flow and the convection regime inside the bends have been examined from Nobari and Gharali [7] numerically as well as from Sobota [8] experimentally. Cvetkovski *et al.* [9] studied on how Dean and Reynolds numbers act in U-bends via CFD analysis with ANSYS. A numerical method has been developed by Yang and Chang [10] for the determination of the convection parameters in curved pipes. Kalb and Seader [11] conducted a numerical investigation for the heat and mass transfer phenomena that take place inside curved circular tubes. Moreover, the convection inside the gap has barely been examined. For example, it has been partially simulated by an alternative way, in study [12], *without* applying air to the gap, while Subiantoro and Tiow [13] presented analytical models for the top heat losses of an FPC and compared them to CFD analysis conducted with ANSYS. The inclination angle effect on the efficiency has, also, been examined experimentally and computationally from Chekerovska and Filkoski [14] by applying tracking system on FPC. The effects of the plate to cover spacing and the inclination angle at the efficiency of a FPC have been studied from Cooper [15]. Apart from the FPC, the concentrating and the evacuated tube systems have, also, been investigated by many researchers [16-21].

In this study the operation of an entire selective FPC with a serpentine flow system is simulated and analyzed. Solidworks and its simulation program *Flow Simulation* were used to design and simulate the whole collector which is the computational domain of this study. The fluids were used are water for pipe flow and air for the gap between the cover and the absorber.

The thermal efficiency, η, of the collector was first calculated. Heat transfer phenomena that take place in the collector were studied for different inlet water temperatures, T_{i}. It is remarkable that however it is difficult to simulate the function of the air in the gap, in our simulation this phenomenon shows quite realistic, since we achieved natural convection to be occurred. In addition, the equivalent heat transfer coefficient between the plate and the cover, $h_{\mathrm{p\text{-}c}}$, was calculated for $\beta = 0°$ and compared to Hollands & Buchberg solutions, respectively, [22-24]. The function of the overall heat loss coefficient, U_{L}, was examined and compared to the Cooper and Dunkle assumption [25, 26]. Moreover, the collector's operation was examined not only in horizontal position but also for 15°, 30°, and 45° inclination angle for 30 °C inlet water temperature. Finally, the secondary flows that occur in the bends of the serpentine tube were examined.

Mathematical bases

In this section the main equations [25] that describe the heat transfer between the parts of the collector as well as between the collector and its environment are presented, in order to understand the system's thermal behavior and the methodology is going to be used in the following analysis.

Equation (1) expresses the heat the water absorbs while eq. (2) provides the overall heat loss coefficient. The top and overall heat losses are given in eqs. (3) and (4) while eq. (5) shows the collector's efficiency. Equation (6) gives the radiative view factor between the plate and the cover [27]:

$$Q_\mathrm{u} = \dot{m}C_p\left(T_o - T_\mathrm{i}\right) = (\tau\alpha)G_T A_\mathrm{c} - U_\mathrm{L} A_\mathrm{c}(T_\mathrm{p} - T_\mathrm{a}) \tag{1}$$

$$U_\mathrm{L} = U_\mathrm{t} + U_\mathrm{b} + U_\mathrm{e} = \frac{Q_\mathrm{t}}{T_\mathrm{p} - T_\mathrm{a}}\frac{1}{A_\mathrm{c}} + \frac{1}{\left(\dfrac{1}{h_\mathrm{w}} + \dfrac{L_\mathrm{b\_ins}}{k_\mathrm{ins}}\right)} + \frac{1}{\left(\dfrac{1}{h_\mathrm{w}} + \dfrac{L_\mathrm{e\_ins}A_\mathrm{c}}{k_\mathrm{ins}A_\mathrm{e}}\right)} \tag{2}$$

$$Q_\mathrm{t} = \left[h_\mathrm{w}\left(T_\mathrm{co} - T_\mathrm{a}\right) + \varepsilon_\mathrm{c}\sigma\left(T_\mathrm{co}^4 - T_\mathrm{a}^4\right)\right]A_\mathrm{c} = h_\mathrm{p\text{-}c}\left(T_\mathrm{p} - T_\mathrm{ci}\right)A_\mathrm{c} + \frac{\sigma\left(T_\mathrm{p}^4 - T_\mathrm{ci}^4\right)}{\dfrac{1}{\varepsilon_\mathrm{p}} + \dfrac{1}{\varepsilon_\mathrm{c}} + \dfrac{1}{F_\mathrm{p\text{-}c}} - 2}A_\mathrm{c} \tag{3}$$

$$Q_\mathrm{L} = U_\mathrm{L} A_\mathrm{c}(T_\mathrm{p} - T_\mathrm{a}) \tag{4}$$

$$\eta = \frac{Q_\mathrm{u}}{A_\mathrm{c}G_T} \tag{5}$$

$$F_\mathrm{p\text{-}c} = \frac{\sqrt{B^2 + 1} - 1}{B} \tag{6}$$

for $L/\delta > 10$, $B = W/\delta$.

The study case

A FPC with a serpentine flow system is simulated and analyzed in detail, fig. 1. The external dimensions of the collector are 1111 × 443 × 96 mm while the height of the air-gap takes the value of 43.3 mm. The design and the components of the examined collector are depicted in fig. 1.

Table 1 gives the material as well as the basic dimensions of the parts that compose the collector while the main properties of the three basic collector's components (cover, absorber and tube, insulation) are shown in tab. 2.

The problem's data are given in tab. 3.

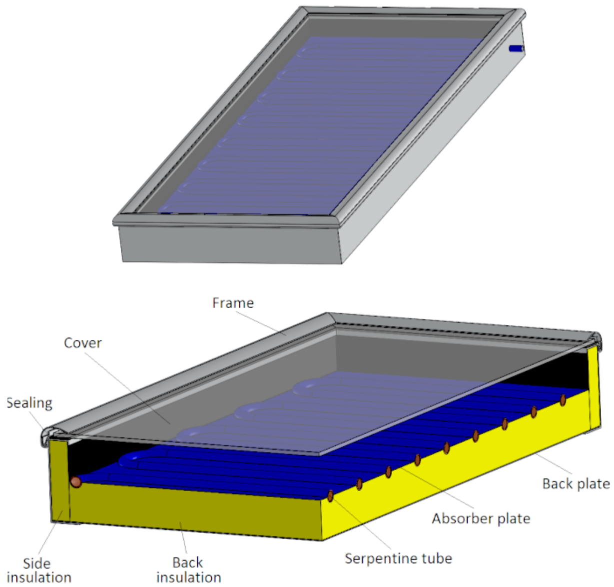

Figure 1. The FPC with serpentine flow system

Table 1. Material and basic dimensions of the collector's components

Component	Material	Thickness [mm]	Other dimensions [mm]
Cover	Low iron glass with antireflective coating	4	Width = 430 , Length = 1098
Absorber plate	Copper	0.2	Width = 400 , Length = 1068
Serpentine tube	Copper	1	D_i = 10 , D_c = 60 , N = 16
Side insulation	Glasswool	20	Along: Length = 1108 Widthwise: Length = 400 Height = 80
Back insulation	Glasswool	40	Width = 400 , Length = 1068
Frame	Aluminum 6063-O	1.5	Along: Outlet length = 1111 Widthwise: Outlet length = 443 Height = 96 Width = 31.5 with 45° chamfer
Sealing	EPDM	2	Along: Outlet length = 1108 Width-wise: Outlet length = 440 Width = 21.5 with 45° chamfer
Back plate	Aluminum 6063-O	0.6	Width = 440 , Length = 1108

Table 2. Optical and thermal properties of the three basic collector's components

Component	Properties
Cover	$\tau = 0.938$, $\varepsilon_c = 0.88$
Absorber & tube	$\alpha = 0.95$, $\varepsilon_p = 0.1$
Insulation	$k_{ins} = 0.04$ W/mK

Table 3. Problem's data

Variable	Value	Units
T_a	10	[°C]
T_i	10-80	[°C]
$\dot{m}$	0.0039	[kgs^{-1}]
h_w	10	[Wm^{-2}K^{-1}]
G_T	800	[Wm^{-2}]

At this point it is essential to mention the assumptions were made, so as to simulate the operation of the collector properly.

First of all, the water flow is considered as laminar, due to the low velocity fields are developed inside the tube, and fully developed, given the small tube diameter relatively to its length. In addition, the optical gain, $(\tau\alpha)$, as well as its surcharge, $0.01(\tau\alpha)$, which is taken because of the multiple reflections of the thermal radiation that occur between the cover and the absorber [26], are defined exclusively from the plate's absorptance coefficient. So, it holds that $\alpha_{sim} = 1.01(\tau\alpha) = 0.9$.

Results

Efficiency of the collector

Figure 2 gives the efficiency and the collector's losses as a function of the variable $(T_i - T_a)/G_T$.

From fig. 2(a) it is obvious that the collector's efficiency decreases by increasing the inlet water temperature, T_i, given that this increment makes indirectly the overall heat losses greater (via T_p increment) and as a consequence causes reduction of the useful energy, Q_u. Figure 2(b) depicts the thermal and optical losses percentage in terms of the available solar energy, respectively.

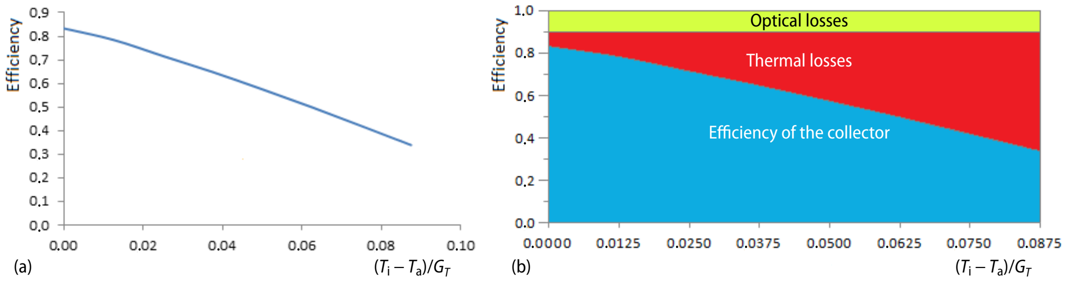

Figure 2. Efficiency and losses of the collector

Overall heat loss coefficient's curve

In fig. 3 that follows two curves of the U_L coefficient as a function of the inlet water temperature, T_i, are presented.

The red curve (1) comes from the first part of eq. (2), while the purple (2) one results from the Cooper and Dunkle assumption via the eq. (7), where a and b are taken from the second order trendline's equation of the efficiency curve:

$$U_L = a + b(T_i - T_a) = 4.543 + 13.599(T_i - T_a) \tag{7}$$

As we can see from fig. 3 there is not a significant difference between these two curves (5% mean divergence) something that reveals how sufficiently the examined physical problem has been approached. In addition, we observe that the U_L coefficient increases with the inlet water temperature, something perfectly reasonable given the collector's components temperature increment.

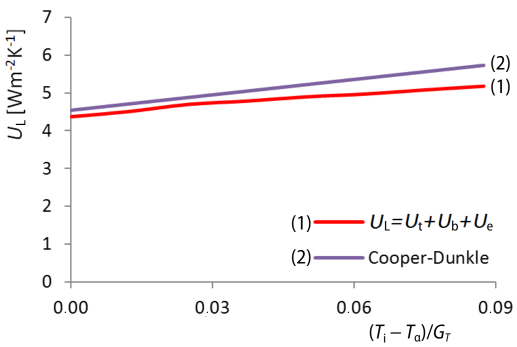

Figure 3. Overall heat loss coefficient's curves

Water, plate, cover, and air temperature curves

Figure 4 depicts the inlet and outlet water temperature curves as well as the average temperature curves of the absorber plate, the inner tube's wall, the water, the cover and the enclosed air as a function of the $(T_i - T_a)/G_T$ parameter.

From fig. 4(a) it becomes obvious that the depicted curves converge as the inlet water temperature, T_i, becomes greater. This happens because the hotter the inlet water is the less the heat it gets from the plate due to the increment of the overall heat losses, eq. (1).

As far as fig. 4(b) is concerned we observe that the curves of T_c, T_{ai}, and T_p diverge among them, something that has to do with the convection that occurs inside the gap as well as with the fact that the cover contacts directly to the cold, relatively to the collector's temperature fields, outer air which does not allow to its temperature rising up rapidly, due to the losses that it adds. It is, also, evident that the $T_p - T_f$ temperature difference is getting lower as the inlet water temperature increases. This reduction represents the reduction of the useful energy, given that the last one can be expressed via this temperature difference, according to eq. (8) that is presented next:

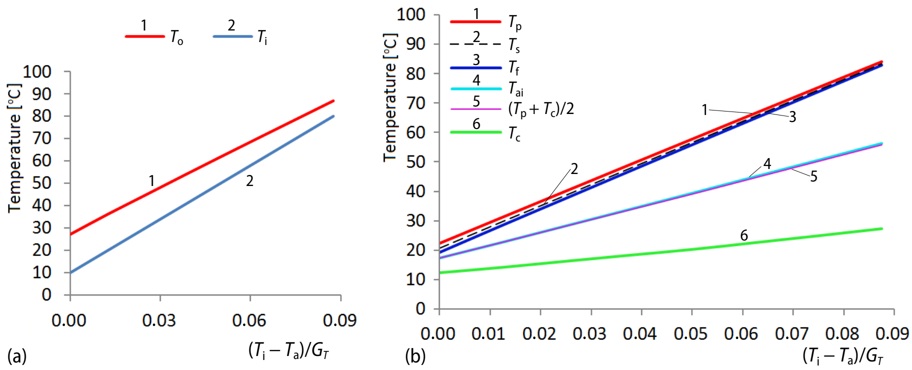

Figure 4. Temperatures (a) inlet and outlet water, (b) average of plate, water, cover, and enclosed air

$$Q_u = \dot{m}C_p(T_o - T_i) = h_f A_s(T_s - T_f) \tag{8}$$

The heat transfer coefficient between the water and the tube, h_f, is getting greater as the water temperature increases. If we, also, take into consideration the reduction of the temperature difference $T_o - T_i$ we conclude that $T_s - T_f$ cannot but being reduced. Hence, $T_p - T_f$ is being reduced too, since T_p and T_s converge as T_i takes higher values.

Water to tube heat transfer coefficient

Given the inner tube wall temperature, T_s, that results from the simulation, it is possible to calculate the water-tube heat transfer coefficient, h_f, via eq. (8), solving for h_f:

$$h_f = \frac{Q_u}{A_s(T_s - T_f)} \tag{9}$$

Figure 8 results from eqs. (9) and (10) as this is presented as:

$$h_{f\_th} = \frac{\mathrm{Nu}_{\mathrm{bend}}\, k_f}{D_i} = \frac{0.913\mathrm{De}^{0.476}\,\mathrm{Pr}^{0.200}\, k_f}{D_i} \tag{10}$$

Valid for $0.7 \le \mathrm{Pr} \le 5$ and $80 \le \mathrm{De} \le 1200$.

$$\mathrm{De} = \mathrm{Re}\sqrt{\frac{R_i}{R_{\mathrm{bend}}}} \tag{11}$$

The eq. (10) can be applied not only for curved tubes but also for piping systems that include bends [11].

As we can see from fig. 5 that follows the h_f coefficient increases with T_i as it was expected. It is, also, observed that the simulation curve approaches sufficiently the theoretical one. More specifically, the theoretical values diverge 12.5% on average from the simulation's ones while the difference between them seems that remains constant as T_i increases.

Tube's centerline water temperature and secondary flows in the bends for T_i = 30 °C

In the fig. 6 the water temperature differentiation on the centerline of the tube, T_{f_center}, with the tube's length is presented.

As it can be seen from fig. 6 the temperature is getting higher gradually at the straight parts of the tube and rapidly at the bends.

These two phenomena are depicted clearly at the following diagram where the temperature fields at a straight part and a bend of the serpentine tube are provided.

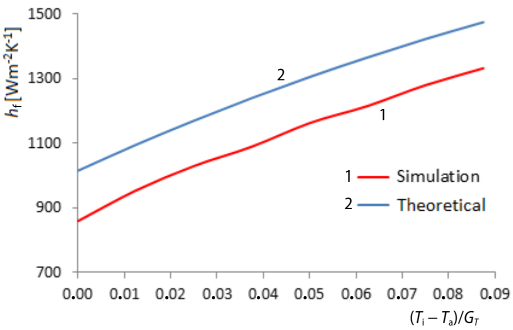

Figure 5. Water to tube heat transfer coefficient's curve

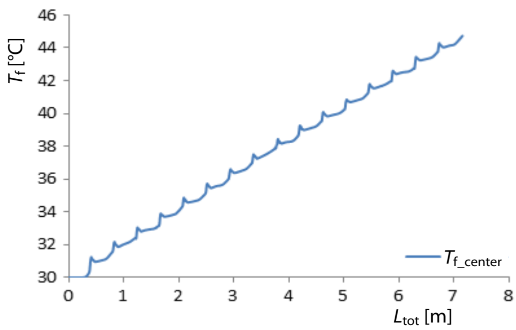

Figure 6. Tube's centerline water temperature

From fig. 7(a) it is observed that the water temperature appears a lag in its increment since its increasing rate is getting higher as we move to the outlet of the straight part. This happens because the heat transfer from the water that wets the tube's walls to the water in the center of the tube requires time to be occurred. The temperature at the entrance seems that decreases due to the flow regime that prevails at the exit of the bend which precedes.

Figure 7(b) shows that the water temperature at the center of the bend increases rapidly while the temperature of the water that wets the walls decreases until approximately the middle of the bend and then rises as the water is been directed to the exit.

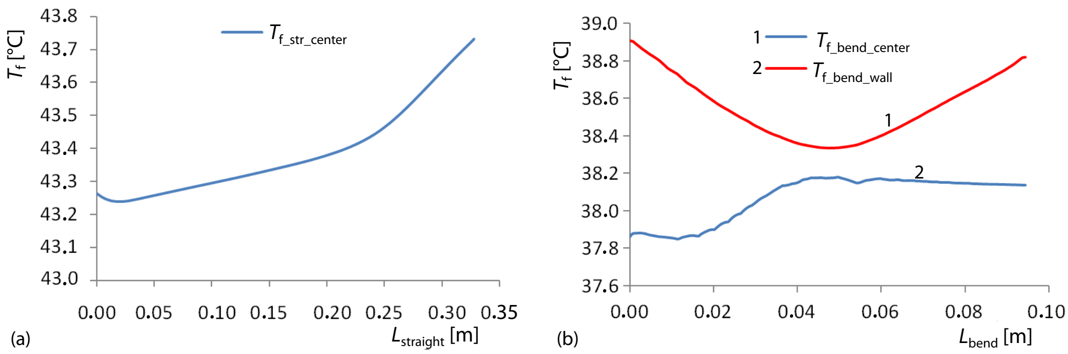

Figure 7. Centerline and top wall line water temperature along the tube; (a) Straight part, (b) Bend

At first sight this phenomenon seems to be complex and difficult to be explained. However, the answer is hidden behind the flow regime that prevails inside the bend. This regime is defined from the secondary flows that take place in there as these are depicted at fig. 8.

Hence, the *cold* water of the center goes to the walls and the *hot* water near the walls goes to the center. According to fig. 8, the whole phenomenon appears higher velocity fields as we go to the exit, while the vortices seem to become weaker since their cores approach the walls.

These secondary flows are being occurred due to the fact that as the water enters the bend the pressure is getting higher at the outer side of it and lower at the inner one due to the inertia forces that exist which are bigger than the viscous ones. This causes the movement of the water particles at the transverse (to the main flow) direction and as a consequence results in the formation of two counter-rotating vortices, the so-called *Dean Vortices* [28], as these are depicted previously, fig. 8.

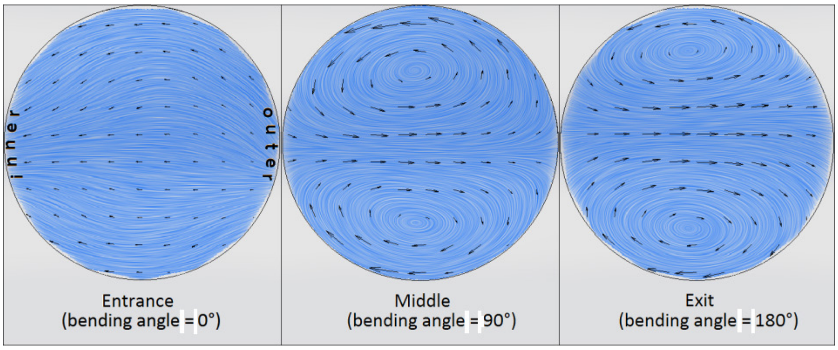

Figure 8. Bend's secondary flows' streamlines for three positions along the main flow

Natural convection in the gap for zero slope

Plate to air and plate to cover heat transfer coefficient ($h_{\text{p–ai}}$, $h_{\text{p–c}}$)

Figure 9(a) that follows results from the simulation and shows the function of plate to enclosed air heat transfer coefficient in terms of the inlet water temperature, T_i.

The plate to cover heat transfer coefficient, fig. 9(b) is being calculated through eq. (3) solving for $h_{\text{p–c}}$ as:

$$h_{\text{p-c, sim}} = \frac{Q_\text{t}}{(T_\text{p} - T_\text{ci})A_\text{c}} - \sigma(T_\text{p}^2 + T_\text{ci}^2)(T_\text{p} + T_\text{ci})\frac{1}{\dfrac{1}{\varepsilon_\text{p}} + \dfrac{1}{\varepsilon_\text{c}} + \dfrac{1}{F_\text{p-c}} - 2} = \frac{\text{Nu}\, k_\text{ai}}{\delta} \tag{12}$$

The particular coefficient is, also, compared to the Buchberg's as well as to the Hollands solution according to the next equations:

$$\text{Nu}_\text{Buchberg} = \begin{cases} 1 + 1.446\left(1 - \dfrac{1708}{\text{Ra}\cos\beta}\right) & \text{for} \quad 1708 < \text{Ra}\cos(\beta) < 5900 \\ 0.229\left(\text{Ra}\cos\beta\right)^{0.252} & \text{for} \quad 5900 < \text{Ra}\cos(\beta) < 9.23\cdot10^4 \\ 0.157\left(\text{Ra}\cos\beta\right)^{0.285} & \text{for} \quad 9.23\cdot10^4 < \text{Ra}\cos(\beta) < 10^6 \end{cases} \tag{13}$$

$$\text{Nu}_\text{Hollands} = 1 + 1.44\left(1 - \frac{1708}{\text{Ra}\cos\beta}\right)\left[1 - \frac{1708\sin^{1.6}(1.8\beta)}{\text{Ra}\cos\beta}\right] + \left[\left(\frac{\text{Ra}\cos\beta}{5830}\right)^{1/3} - 1\right] \tag{14}$$

$$\text{Ra} = \frac{g\beta' \Delta\text{T}_\text{p-c}\delta^3}{\nu a} \tag{15}$$

From fig. 9(a) it is observed that the convection in the plate-air interface becomes weaker with T_i increment and stable for $T_i \geq 30$ °C. This phenomenon has to do with the way that convection occurs between the air and the plate. In particular, there are two driving forces that contribute in the plate to air convection. The first one is the $T_p - T_c$ temperature difference that causes the transversal convection (air movement from plate to cover and conversely) while the second one is $T_{p\_max} - T_{p\_min}$ which in turn causes the longitudinal convection (air movement from the coldest part of the collector to the hottest and conversely). The last one is getting weaker by increasing T_i due to the reduction of $T_{p\_max} - T_{p\_min}$ while the first becomes stronger due to the $T_p - T_c$ increment. This two phenomena seems to cancel each other in the plate-air interface for $T_i \geq 30$ °C. So, fig. 9(a) depicts the effect of the combination of these two convections on plate to air interface.

We observe, through fig. 9(b), that the present simulation approaches sufficiently the other two solutions. In particular, the mean divergences are 7% from Buchberg's and 14% from Hollands solution. It is, also, obvious that the h_{p-c} coefficient increases something that happens due to the increment of the plate to cover temperature difference which makes the Nusselt number higher through the Raleigh number as T_i increases.

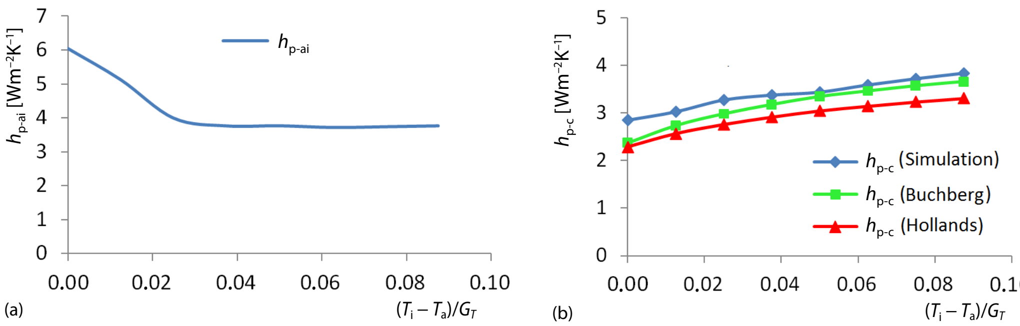

Figure 9. Heat transfer coefficients; (a) plate-air, (b) plate-cover (simulation, Buchberg, Hollands)

Diagrams and allocations for T_i = 30 °C and β = 0°, 15°, 30°, and 45°

Figure 10 depicts how h_{p-c}, h_{p-ai} and the efficiency, η, change as a function of the inclination angle.

As it is depicted on fig. 10(a) the heat transfer coefficients are getting reduced as β increases. This happens due to the fact that as the slope becomes greater the natural convection is getting weaker because the hot air is being trapped near to the higher part of the gap while the cold one stays down. From fig. 10(b) it is obvious that the greater the tilt is the more efficiently the collector operates something that occurs due to the reduction of the top heat losses which in turn is caused from the plate to cover heat transfer coefficient reduction as we saw in fig. 10(a).

At the fig. 11 the air temperature distribution at the *cold* part of the collector is depicted as a function of the inclination angle.

As we can see from fig. 11 the air temperature in this specific area of the collector is getting reduced as the slope becomes greater because the cold air is being increasingly gathered at the bottom of the gap. Figure 12 depicts how natural convection takes place in the gap. The hot and the cold air is directed to the cover and the plate, respectively, as it was expected leading to the formation of several vortices inside the gap.

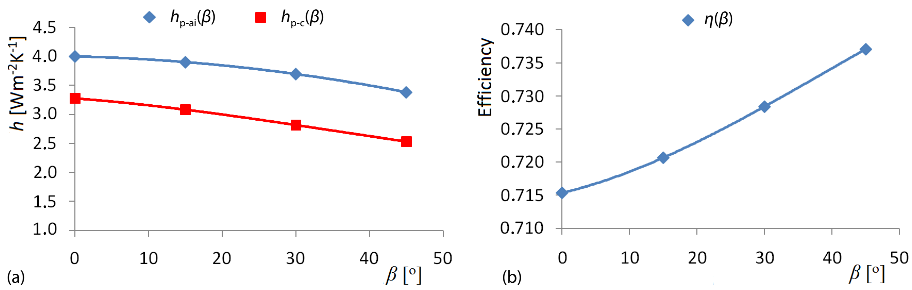

Figure 10. (a) Plate-cover and plate-air heat transfer coefficients, (b) efficiency dependent on the slope

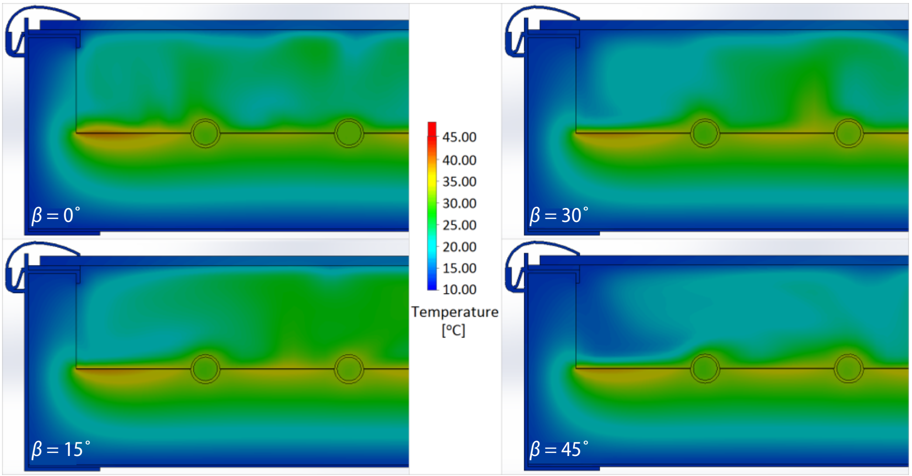

Figure 11. Air temperature near the inlet as a function of the slope for T_i = 30 °C (*for color image see journal web site*)

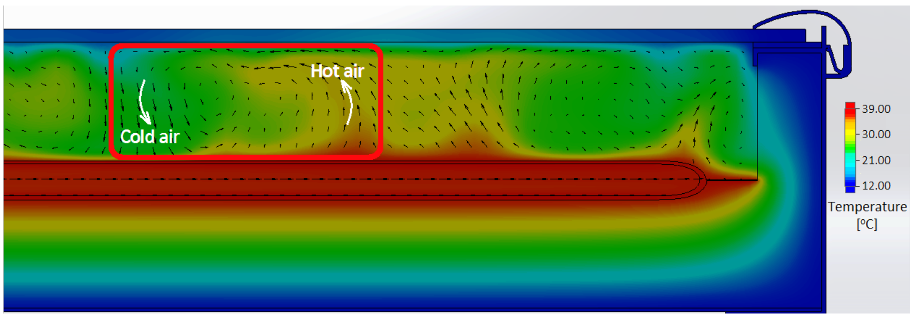

Figure 12. Enclosed air natural circulation at the middle of the collector for T_i = 30 °C and β = 0° (*for color image see journal web site*)

Figure 13 that follows depicts the absorber's temperature range from the inlet to the outlet.

From fig. 13(a) it can be seen that the plate temperature is getting higher as the water is been directed from the inlet to the outlet of the collector in the *Y*-direction. This happens because the warmer the water is the less the heat is taken from the plate.

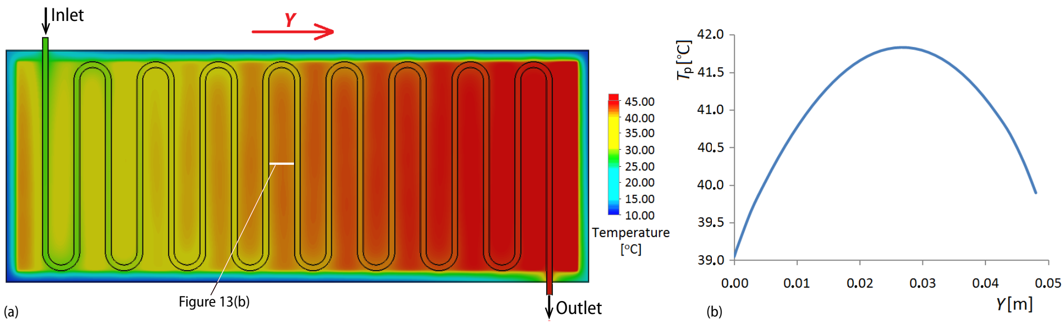

Figure 13. (a) Absorber plate's temperature fields for T_i = 30 °C and β = 0° (b) absorber plate's temperature along the line is depicted at fig. 13(a) in the Y-direction
(*for color image see journal web site*)

It, also, becomes obvious, figs. 13(a) and 13(b) that the plate temperature between two straight serpentine segments takes its lower values near the tube and its higher ones approximately at the middle of the distance between the segments, something that declares the role the water plays in the specific case which is none other than a heat sink hole.

Conclusions

In this paper the thermal operation of a serpentine FPC was examined while the flow and the convection regime inside the tube and the gap were determined and analyzed in detail. Next the most important concluding remarks resulted from this study are reported.

- The water to tube heat transfer coefficient, fig. 5, was validated and found to diverge from theory approximately 12.5% on average.
- Figure 6 declares the existence of the secondary flows which are caused by the inertia forces exerted on the water as this enters the bend owing to the abrupt direction change.
- The air circulation inside the gap is a combination of the transversal and the longitudinal convection which resulted from $T_p - T_c$ and $T_{p\_max} - T_{p\_min}$ temperature differences, respectively.
- The plate to cover heat transfer coefficient, h_{p-c}, increases with T_i because the $T_p - T_c$ temperature difference is getting greater while the mean divergence of it from Buchberg's and Hollands solutions was 7% and 14%, respectively, fig. 9(b).
- The inclination angle, β, plays a significant role at the efficiency of the collector since its increment results in a lower convection regime inside the gap, fig. 10(a), and as a consequence a greater efficiency can be achieved, fig. 10(b).
- As the slope increases the hot air to cover interface becomes smaller and as a result less hot air is being cooled from the cover. This in combination with the entrapment of the hot and the cold air at the higher and the lower part of the collector respectively due to the gravity forces, fig. 11, causes the suppression of the convection inside the gap.

Acknowledgement

The first author would like to thank Bodossakis Foundation for its financial support.

Nomenclature

A – surface area, [m^2]
a – thermal diffusivity, [m^{2}s^{-1}]
C_p – fluid specific heat, [kJkg^{-1}K^{-1}]
D – diameter, [m]
De – Dean number [= Re$(R_i/R_{bend})^{1/2}$], [–]
F – view factor, [–]
G_T – global irradiance, [Wm^{-2}]
g – gravity acceleration, [ms^{-2}]

h – convective heat transfer coefficient, [$Wm^{-2}K^{-1}$]
k – thermal conductivity, [$Wm^{-1}K^{-1}$]
L – length, [m]
$\dot{m}$ – mass-flow rate, [kgs^{-1}]
N – number of bends, [–]
Nu – Nusselt number (= hD/k), [–]
Pr – Prandtl number (= ν/a), [–]
Q – heat flux, [W]
R – radius, [m]
Ra – Raleigh number [= $g\beta'\Delta T_{p-c}\delta^3(\nu a)^{-1}$], [–]
Re – Reynolds number (= UD/ν), [–]
U – heat loss coefficient, [$Wm^{-2}K^{-1}$]
W – plate's width, [m]
T – temperature, [°C]

Greek symbols

α – absorptivity, [–]
β – inclination angle, [°]
β' – volumetric coefficient of expansion, [K^{-1}]
δ – cover to plate distance, [m]
ε – emissivity, [–]
η – efficiency, [–]
ν – kinematic viscosity, [m^2s^{-1}]
σ – Boltzmann constant, [$Wm^{-2}K^{-4}$]
τ – transmittance, [–]

Subscripts

a – ambient
ai – enclosed air
b – bottom
bend – bend
c – cover
ci – inner cover surface
co – outer cover surface
e – side
f – water
i – inner (for *D*), inlet (for *T*)
ins – insulation
L – overall
o – outer (for *D*), outlet (for *T*)
p – plate
p-ai – plate to enclosed air
p-c – plate to cover
s – tube's walls
sim – simulation
str – straight serpentine segment
t – top
tot – total for tube's length
u – useful
w – wind

References

[1] Zabara, K., Estimation of the Global Solar Radiation in Greece, *Solar & Wind Technology*, *3* (1986), 4, pp. 267-272
[2] Kouremenos, D. A., *et al.,* Solar Radiation Correlations for the Athens Area, Greece, *Solar Energy*, *35* (1985), 3, pp. 259-269
[3] Kalogirou, S. A., Solar Thermal Collectors and Applications, *Progress in Energy and Combustion Science*, *30* (2004), 3, pp. 231-295
[4] Lior, N., *Thermal Theory and Modeling of Solar Collectors*, MIT Press, Cambridge, Mass., USA, 1990
[5] Eisenmann, W., *et al.*, *Experimental Investigations of Serpentine-Flow Flat-Plate Collectors*, Philipps University Marburg, Marburg, Germany
[6] Cook, Z. A., Retrofitting Two Solar Hot Water Systems for Year Round Operation: All Graduate Plan B and other Reports, Report No. 372, Utah State University, Logan, Ut., USA, 2014
[7] Nobari, M. R. H., Gharali, K., A Numerical Study of Flow and Heat Transfer in Internally Finned, *International Journal of Heat and Mass Transfer*, *49* (2006), 5-6, pp. 1185-1194
[8] Sobota, T., Experimental Prediction of Heat Transfer Correlations in Heat Exchangers, in: *Developments in Heat Transfer* (Ed. M. A. D. S. Bernardes), *In Tech*, Rijeka, Croatia, 2011, pp. 294-308
[9] Cvetkovski, C. G., *et al*., Heat Transfer in a U-Bend Pipe; Dean Number versus Reynolds Number, *Sustainable Energy Technologies and Assessments*, *11* (2015), Sept., pp. 148-158
[10] Yang, R, Chang, S. F., Combined Free and Forced Convection for Developed Flow in Curved Pipes with Finite Curvature Ratio, *International Journal of Heat and Fluid Flow*, *15* (1994), 6, pp. 470-476
[11] Kalb, C. E., Seader, J. D., Heat and Mass Transfer Phenomena for Viscous Flow in Curved Circular Tubes, *Heat and Mass Transfer*, *15* (1972), 4, pp. 801-817
[12] Bellos, E., *et al.*, Thermal Analysis of a Flat Plate Collector with Solidworks and Determination of Convection Heat Coefficient between Water and Absorber, *Proceedings*, 28th International Conference on Efficiency, Cost, Optimization, Simulation, and Environmental Impact of Energy Systems, Pau, France, 2015
[13] Subiantoro, A., Tiow, O. K., Analytical Models for the Computation and Optimization of Single and Double Glazing Flat Plate Solar Collectors with Normal and Small Air Gap Spacing, *Applied Energy*, *104* (2013), Apr., pp. 392-399

[14] Chekerovska, M., Filkoski, R. V., Efficiency of Liquid Flat-Plate Solar Energy Collector with Solar Tracking System, *Thermal Science, 19* (2015), 5, pp. 1673-1684
[15] Cooper, P. I., The Effect of Inclination on the Heat Loss from Flat-Plate Solar Collectors, *Solar Energy*, *27* (1981), 5, pp. 413-420
[16] Korres, D. N., Tzivanidis, C., Optical and Thermal Analysis of a New U-Type Evacuated Tube Collector with a Mini-Compound Parabolic Concentrator and a Cylindrical Absorber, *Proceedings*, 29th International Conference on Efficiency, Cost, Optimization, Simulation, and Environmental Impact of Energy Systems, Portoroz, Slovenia, 2016
[17] Korres, D. N., *et al.,* Thermal and Optical Investigation of a U-Type Evacuated Tube Collector with a Mini-Compound Parabolic Concentrator and a Flat Absorber, *Proceedings*, 7th International Conference from "Scientific Computing to Computational Engineering", Athens, Greece, 2016
[18] Tzivanidis, C., *et al.,* Thermal and Optical Efficiency Investigation of a Parabolic trough Collector, *Case Studies in Thermal Engineering*, *6* (2015), Sept., pp. 226-237
[19] Chen, M., Performance Comparison of a New-Type Rough Solar Concentrator Thermal System in Different Installations, *Thermal Science*, *19* (2015), Suppl. 2, pp. S535-S545
[20] Bellos, E., *et al.,* Design, Simulation and Optimization of a Compound Parabolic Collector, *Case Studies in Thermal Engineering*, *20* (2015), Aug., pp. 53-63
[21] Pavlović, S., *et al*., Optical Modeling of Solar Dish Thermal Concentrator Based on Square Flat Facets, *Thermal Science*, *18* (2014), 3, pp. 989-998
[22] Nahar, N. M., Garg, H. P., Free Convection and Shading Due to Gap Spacing between an Absorber Plate and the Cover Glazing in Solar Energy Flat-Plate Collectors, *Applied Energy*, *7* (1980), 1-3, pp. 129-145
[23] Buchberg, H., *et al.*, Natural Convection in Enclosed Spaces – A Review of Applications for Solar Energy Collection, *Heat Transfer*, *98* (1976), 2, pp. 182-188
[24] Hollands, K. G. T., *et al.*, Free Convective Heat Transfer Across Inclined Air Layers, *Heat Transfer*, *98* (1976), 2, pp. 189-193
[25] Cooper, P. I., Dunkle, R. V., A Non-Linear Flatplate Collector Model, *Solar Energy, 26* (1981), 2, pp. 133-140
[26] Duffie, J., Beckmann, W., *Solar Engineering of Thermal Processes,* John Wiley and Sons Inc., 2nd ed., New York, USA, 1991
[27] Theodore, L., *et al.*, *Fundamentals of Heat and Mass Transfer,* John Wiley and Sons Inc., 7th *ed.*, , New York, USA, 2011
[28] Carlsson, C, *Heat Transfer in Curved Pipes*, Lunds University, Lund, Sweden, 2014

Paper submitted: November 30, 2016
Paper revised: March 13, 2018
Paper accepted: May 13, 2018